THE BELL SYSTEM TECHNICAL JOURNAL
Vol. 58, No. 4, April 1979
Printed in U.S.A.

Rapid Automatic Index Profiling of Whole-Fiber Samples: Part II

By H. M. PRESBY, D. MARCUSE, H. W. ASTLE, and L. M. BOGGS

(Manuscript received May 1, 1978)

Automatic, nondestructive methods have been developed for measuring and analyzing the refractive index distribution of a fiber that is immersed in index-matching oil and illuminated transversely to its axis in a single-pass interference microscope. The output field of the microscope is automatically processed with a video-digitized, computer-controlled system, and the profile is determined by the solution of an integral equation that can handle arbitrary variations in the index distribution. The resulting profiles are reproducible to approximately 1 percent and can be determined within a few minutes after fiber fabrication. Details of a rapid video scanning procedure and of error estimates involved in solving the integral equation are presented along with representative profiles.

I. INTRODUCTION

One of the most important parameters in determining the usefulness of graded-index multimode optical fibers in high-capacity communication systems is their refractive index profile. The closer the profile conforms to the required optimum distribution, the greater the resulting bandwidth of the fiber. As demand for high-capacity fibers increases and as fabrication facilities are optimized to produce them dependably, it becomes very important to have reliable, accurate, and fast methods to measure the fiber's refractive index distribution. These methods would greatly aid in tailoring more ideal profiles and would form the basis of a fiber evaluation and sorting scheme in which fibers are selected for specific applications, depending upon the quality of their profiles, almost immediately upon production.

One of the most sensitive means of measuring the index profile is by interference microscopy utilizing cut and polished fiber-slab samples.[1,2] While this technique allows very precise measurements,[3,4] it requires

a high precision, time-consuming procedure of preparing the thin (on the order of 50 μm) and extremely flat samples. This can be alleviated somewhat by simultaneously processing many samples and utilizing an automatic analysis scheme to save time in the evaluation;[5,6] however, it would still be preferable to avoid any sample preparation.

A technique requiring no sample preparation based on interferometry has been proposed in which a sample of the whole fiber is immersed in index-matching oil and illuminated perpendicular to its axis.[7] The refractive index profile is subsequently obtained from the fringe shifts by mathematical methods which were shown to operate for fibers whose profiles are a quadratic function of the radius of the core. This method has also been extended[8] to a more general class of profile shapes describable by a parameter α which appears in the expression describing the index distribution $n(r)$,

$$n(r) = n_0[1 - 2\Delta(r/a)^\alpha]^{1/2},$$

where r is the distance from the center of the core, a is the core radius, and $\Delta n \equiv n_o - n_a$. Assuming that α is constant, this treatment showed that Δn and α could be determined to better than ± 10 percent. The assumption of constant α, however, is a severe restriction not met by most currently fabricated fibers and the resulting accuracy of ± 10 percent is also not sufficient for many applications. In addition, these methods cannot accommodate arbitrary perturbations of the profile which commonly exist in the form of barrier layers at the core-cladding interface and an index depression along the axis of the fiber.

These limitations have been overcome with a method of analysis in which profiles with arbitrary shapes can be handled.[9] In that analysis, the fiber core is modeled as having many layers, with each layer having a constant index of refraction. The profile is then built up in a stepwise manner using the index value from each preceding section as the starting point for the next. The resulting accuracy is on the order of a few percent.

That analysis, however, is based on having a certain minimum width for each layer and breaks down if smaller intervals are utilized. While this is not a serious limitation in practice, it may present problems if very rapid and narrow variations occur in the profile. We have therefore developed a new analysis scheme not having this potential drawback in which the profile is obtained by the solution of an integral equation which can handle small regions. However, this new method is still restricted to index profiles of rotational symmetry. We have also fully automated the measurement and analysis procedure so that its inherent rapid nature can be fully exploited. We call our nondestructive measuring procedure the "whole-fiber method."

This paper consists of two basic sections. In the first, the details of the solution of the integral equation and error estimates are treated.

In the second, the automated system is described and various profiles are presented, discussed, and compared with those obtained by other methods.

II. SOLUTION OF THE INTEGRAL EQUATION AND ERROR ESTIMATE

In the whole-fiber method, the ray traverses the fiber core at right angles to its axis.[8] The phase shift of each ray is an integral over the product of the length element of the ray path ds times the relative refractive index (relative with respect to the cladding index n_c). Ignoring ray bending in the core, we may express the relative phase shift according to Fig. 1 as

$$P(r) = \frac{4\pi}{\lambda} \int_r^\infty [n(\rho) - n_c] \frac{\rho d\rho}{\sqrt{\rho^2 - r^2}}. \tag{1}$$

The upper limit of the integral actually need only be $\rho = a$ but, because $n(\rho) = n_c$ for $\rho > a$, we may as well use the limit ∞. To obtain the relation between the fringe shift $S(r)$ and the relative phase shift P, we observe that the ratio of fringe shift to fringe spacing D must be equal to the ratio of the relative phase shift to 2π,

$$\frac{S(r)}{D} = \frac{P(r)}{2\pi}. \tag{2}$$

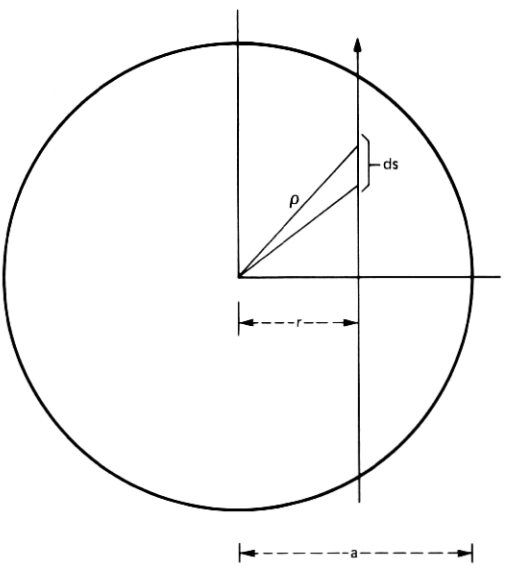

Fig. 1—Outline of fiber core and variables appearing in eq. (1).

Equations (1) and (2) thus lead to the following integral equation for $n(\rho) - n_c$:

$$\int_r^\infty [n(\rho) - n_c] \frac{\rho d\rho}{\sqrt{\rho^2 - r^2}} = \frac{\lambda}{2D} S(r). \tag{3}$$

We show in the appendix that the solution of this integral equation may be expressed as

$$\Delta n(r) = n(r) - n_c = -\frac{\lambda}{\pi D} \int_r^\infty \frac{dS(\rho)}{d\rho} \frac{d\rho}{\sqrt{\rho^2 - r^2}}. \tag{4}$$

This explicit solution of the integral equation (3) shows that the refractive index difference at any point r in the fiber core can be obtained from a knowledge of the fringe shift function $S(r)$ by differentiation and integration. Since the fringe shift is known only at certain discrete points, numerical techniques [see eq. (14)] for approximating the derivative as well as the integral must be used.* The accuracy of the resulting refractive index distribution depends on the accuracy of the measurement of $S(r)$, on the density of points at which $S(r)$ is being measured, and on the sophistication of the methods used for numerical evaluation.

The explicit solution (4) of the integral equation (3) is useful not only for obtaining numerical solutions for the refractive index profile but also for calculating estimates of the error of Δn that is introduced by the fact that the measured values of the fringe shift $S(r)$ are only known to a limited precision. We use the subscript o to indicate the index difference Δn_o that would be obtained if the fringe shift S_o and its derivative were known precisely. The variance of the refractive index difference is thus, according to (4),

$$\langle (\Delta n - \Delta n_o)^2 \rangle$$

$$= \left(\frac{\lambda}{\pi D}\right)^2 \int_r^\infty d\rho \int_r^\infty d\rho' \frac{\langle [\dot{S}(\rho) - \dot{S}_o(\rho)][\dot{S}(\rho') - \dot{S}_o(\rho')] \rangle}{\sqrt{(\rho^2 - r^2)(\rho'^2 - r^2)}}. \tag{5}$$

The derivative of S is indicated by the notation $\dot{S}$ and the symbol $\langle\ \rangle$ designates an ensemble average. The numerator under the integral sign in (5) is the autocorrelation function of the derivative of the fringe shift S. For simplicity, we assume that this function is of the following form:

* At and near $\rho = r$, an analytical approximation of (4) is used, based on a fourth-order polynomial expansion of $S(\rho)$.

$$R_d = <[\dot{S}(\rho) - \dot{S}_o(\rho)][\dot{S}(\rho') - \dot{S}_o(\rho')]>$$

$$= \begin{cases} (\Delta\dot{S})^2 & \text{for } |\rho - \rho'| < B \\ 0 & |\rho - \rho'| > B. \end{cases} \quad (6)$$

The autocorrelation function is assumed to have a constant value, equal to the variance of the function $\dot{S}$, over a narrow region outside of which it vanishes. The interval B assumes the physical meaning of a correlation length. We consider B as a very short distance, much shorter than any of the transverse dimensions of the fiber. This assumption allows us to work out the following approximation for (5).

$$<(\Delta n - \Delta n_o)^2> = \left(\frac{\lambda}{\pi D}\right)^2 (\Delta\dot{S})^2 \frac{B}{r} \ln\left(\frac{2r}{B}\right). \quad (7)$$

Approximation (7) is valid only for $r \gg B$; however, if we try to evaluate (5) with the special function (6) directly at $r = 0$ we find an infinite result. This failure indicates that it is not permissible to use (6) for arbitrarily small values of ρ because the derivative of S, and hence its variance, must vanish at $\rho = 0$ because of the symmetry of the structure. Assuming $(\Delta\dot{S})^2$ to be constant is thus not permissible for arbitrarily small values of ρ.

The variance $(\Delta\dot{S})^2$ of the derivative of the fringe shift function S is not easy to visualize intuitively. For this reason, we must relate it to the variance $(\Delta S)^2$ of the fringe shift function itself. The autocorrelation function (6) for $\dot{S}$ and the autocorrelation function for S

$$R(u) = <[S(\rho) - S_o(\rho)][S(\rho + u) - S_o(\rho + u)]> \quad (8)$$

are related by the well-known equation[11]

$$R_d = -\frac{d^2R}{du^2}. \quad (9)$$

If we exclude the point $|u| = B$, and keep in mind that $R(u) = R(-u)$ is required, we conclude that if R_d has the form (6) R must have the functional form

$$R(u) = \begin{cases} (\Delta S)^2 \dfrac{B^2 - u^2}{B^2} & \text{for } |u| < B \\ 0 & \text{for } |u| > B. \end{cases} \quad (10)$$

Equations (6), (9), and (10) lead to the following relation between the variance $(\Delta\dot{S})^2$ of the derivative of the fringe shift function and the variance $(\Delta S)^2$ of the fringe shift function itself:

$$(\Delta\dot{S})^2 = \frac{2(\Delta S)^2}{B^2}. \quad (11)$$

Substituting (11) into the square root of (7) finally yields the following expression for the rms deviation of the refractive index difference:

$$\delta[\Delta n(r)] = \frac{\sqrt{2}\,\lambda\Delta S}{\pi D}\left[\ln\frac{2r}{B}\right]^{1/2}, \tag{12}$$

with the definition

$$\delta(\Delta n) = [<(\Delta n - \Delta n_o)^2>]^{1/2}. \tag{13}$$

It remains to obtain an estimate for the correlation length B. We assume that the measured values of the fringe shift S at equidistantly spaced measuring points r_i are used to define a Lagrange interpolation polynomial

$$F = \sum_{i=1}^{n+1}\prod_{\substack{j=1\\ \neq i}}^{n+1}\left(\frac{r - r_j}{r_i - r_j}\right) S_i, \tag{14}$$

where we used the abbreviation

$$S_i = S(r_i). \tag{15}$$

An interpolation polynomial of this type with $n = 4$ is actually used to evaluate the derivative $\dot{S}$ and the integral in (4). We assume that the differences of the measured values S_i and the true values $S_o(r_i)$ are mutually uncorrelated,

$$<(\Delta S_i)(\Delta S_j)> = (\Delta S_i)^2\delta_{ij}, \tag{16}$$

where, by definition,

$$\Delta S_i = S_i - S_o(r_i). \tag{17}$$

We use $n + 1$ adjacent points r_i to define F according to (14) and extend this function outside this range by defining a new function with the help of the next set of $n + 1$ adjacent points, etc. Using

$$R_F(u) = <\Delta F(r)\Delta F(r + u)>, \tag{18}$$

where ΔF is defined in analogy with (17),

$$\Delta F = F(r) - F_o(r), \tag{19}$$

we have computed the function (18) numerically by using (14) and (16). Figures 2 through 5 show the results of these computations for a few points $r = 1$, 1.5, 2, and 2.5 for a fourth-order polynomial approximation using points $r_1 = 1$ through $r_5 = 5$ and extend this function by corresponding polynomials outside of this range. The endpoints of one range are simultaneously also endpoints of the polynomial expansions in adjacent ranges. It is apparent that the autocorrelation function is neither stationary nor symmetric because it depends on the choice of

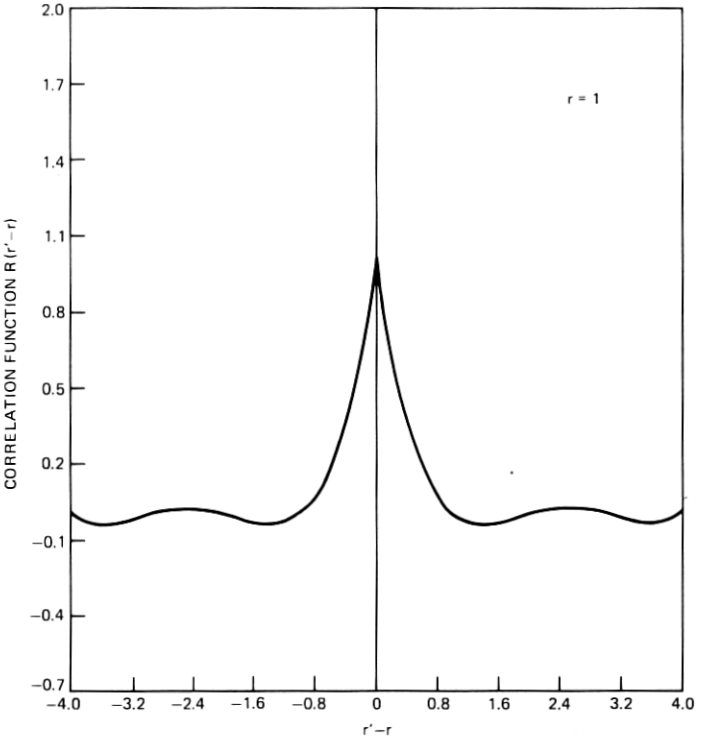

Fig. 2—Correlation function $R(r' - r)$ associated with a fourth-order interpolation polynomial if the functional values at the five points used to define the interpolation polynomial are mutually uncorrelated. The distance between adjacent interpolation points is used as the unit of length. In this figure, the autocorrelation function is evaluated with $r = 1$ being the end point of adjacent interpolation intervals. Adjacent intervals (of 5 points each) are approximated by similar interpolation polynomials. Note that, for this choice of r, the function assumes a symmetrical appearance.

r in (18). On the other hand, we may use this approach to gain an order-of-magnitude estimate of the correlation length B. Figure 6 shows an average of the autocorrelation functions averaged over r. This function is very nearly of the form $(\sin x)/x$ and, in its central portion, is a reasonable order-of-magnitude approximation of the correlation function (10). It is clear from this averaged autocorrelation function that the correlation length B is on the order of the length of the interval used for defining the individual interpolation function,

$$B = n\Delta r, \tag{20}$$

where Δr indicates the distance between adjacent sampling points

$$\Delta r = r_{i+1} - r_i. \tag{21}$$

Even though our error analysis can claim to give no more than an order-of-magnitude estimate, (12) and (20) show that the error due to

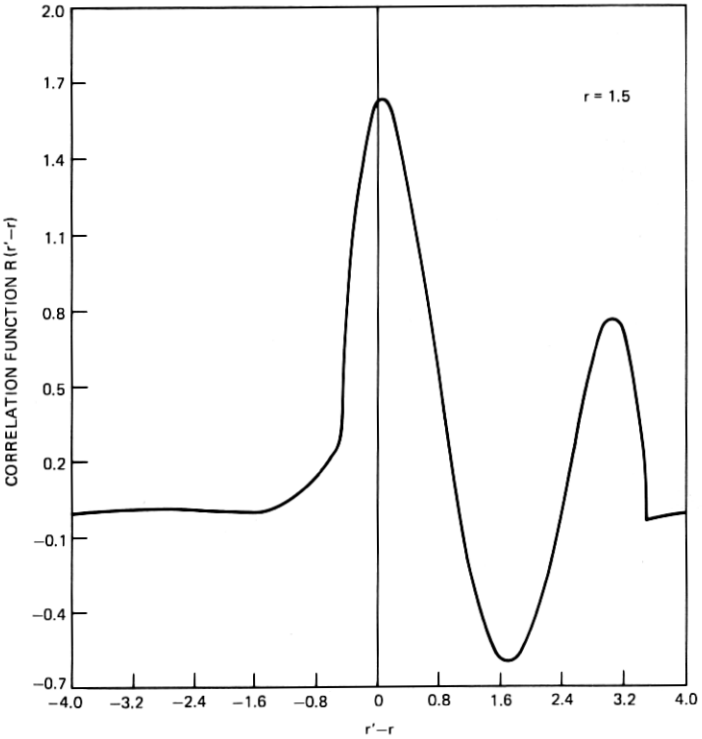

Fig. 3—Similar to Fig. 2 with $r = 1.5$. The autocorrelation function is now not symmetrical around the point $r' - r = 0$.

the limited accuracy of the measurements of the fringe shift $S(r)$ increases as r decreases and also that the error of the refractive index determination increases as the length of the interval Δr between adjacent sampling points decreases. This latter error can be decreased by using an interpolation polynomial of higher order. All these trends have been clearly observed in our experimental results.

To gain insight into the numerical values of the rms deviation $\delta(\Delta n)$, let us make the following assumptions. The distance between adjacent scan lines of the vidicon corresponds to 0.2 μm of the vertical direction along the fiber core. Because of an averaging procedure using 10 adjacent scan lines for finding the center of each fringe, we may assume $\Delta S = 0.2/10 = 0.02$ μm. The distance between adjacent sampling points in horizontal direction is typically $\Delta r = 1$ μm. We set $n = 4$ because of our use of a fourth-order interpolation polynomial. The fringe spacing is typically $D = 6$ μm. If we use $\lambda = 1$ μm and use a value halfway between core center and core boundary, $r = 15$ μm, we find, from (12),

$$\delta(\Delta n) = 3 \times 10^{-4}. \tag{22}$$

This amount of rms deviation is in excellent agreement with the

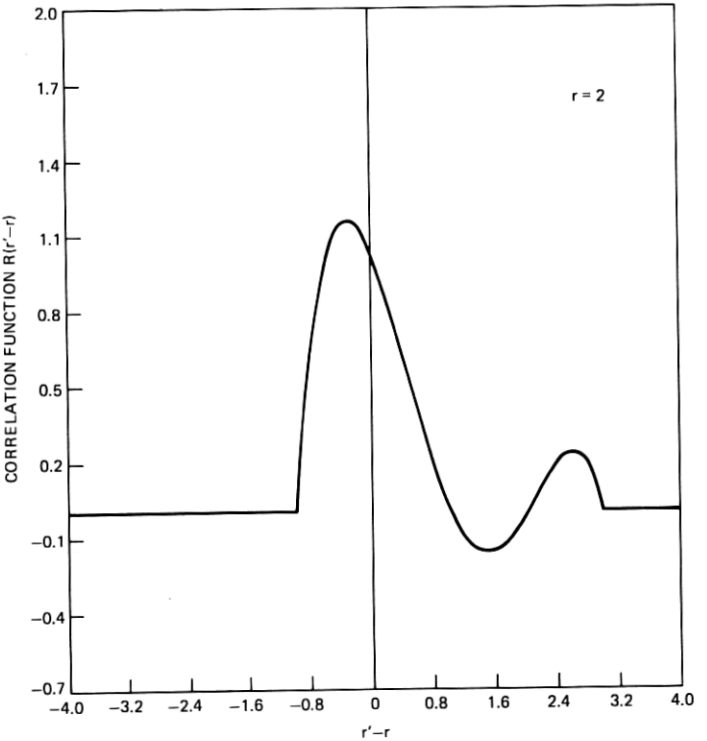

Fig. 4—Similar to Figs. 2 and 3 with $r = 2$.

observed values. However, it is important to remind the reader that this is the error caused by the random uncertainty in the fringe position that is inherent in the measuring process. It is not the absolute error relative to the (unknown) precise value of Δn. Our derivation of the error estimate (12) is limited to the random component of the uncertainty of the fringe shift S and does not include systematic errors arising from distortions in the imaging process of the microscope or the vidicon and furthermore does not include the systematic error arising from the process of using a finite number of discrete points for evaluating the derivative $\dot{S}$ and the integral in (4). Only the additional error caused by the uncertainty about the actual values of $S(r_i)$ at the sampling points is responsible for the rms deviation of Δn expressed by (12). Systematic errors existing in the system have been investigated, however, and were found to be at least one order of magnitude less than this value.

III. AUTOMATIC PROCESSING AND ANALYSIS SYSTEM

The experimental arrangement to automatically measure and analyze the profiles of whole fibers is shown in Fig. 7. The use of this

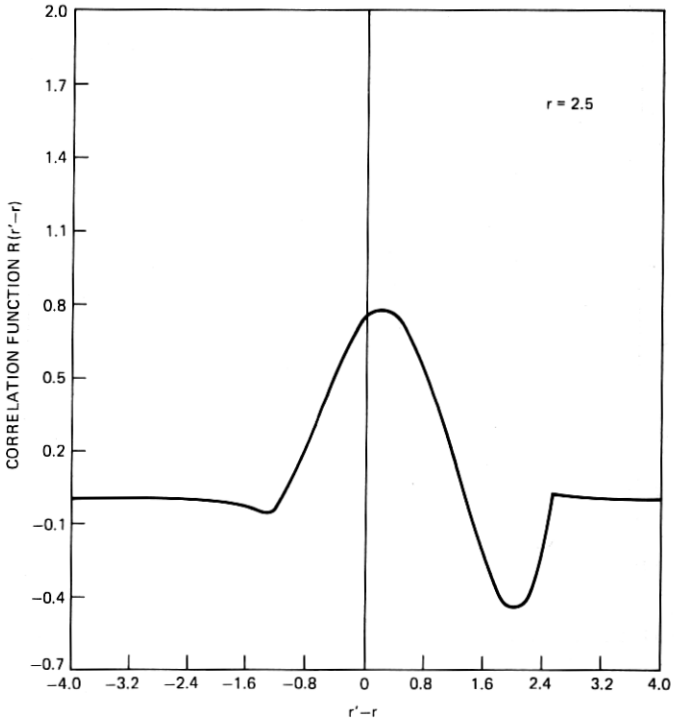

Fig. 5—Similar to Figs. 2 and 3 with $r = 2.5$.

system has been briefly described elsewhere.[9] Here, we discuss the full details of its operation.

The basis of the system is a Leitz dual-beam, single-pass transmission interference microscope which is generally used to perform precise refractive index profiling of optical fibers by examining polished slab samples.[1-6] For the whole-fiber measurements, a short length of fiber (~1 cm) is inserted into index-matching oil in the sample arm of the microscope and a similar thickness of oil is placed in the reference beam. An excellent match to the cladding could be achieved at an observation wavelength $\lambda = 0.9$ μm with matching oil of index $n_D = 1.457 \pm 0.0005$ with no temperature control.

The output field of the microscope is detected with an infrared-enhanced, silicon-target vidicon, and the video signal is sent to a video digitizer that has the capability of addressing discrete picture elements in the television frame and digitally encoding the intensity at each element. The digitizer resolves 480 picture elements along the Y axis and 512 elements on the X axis. The X- and Y-position data inputs are provided by the 16-bit duplex input/output (I/O) interfaces of a

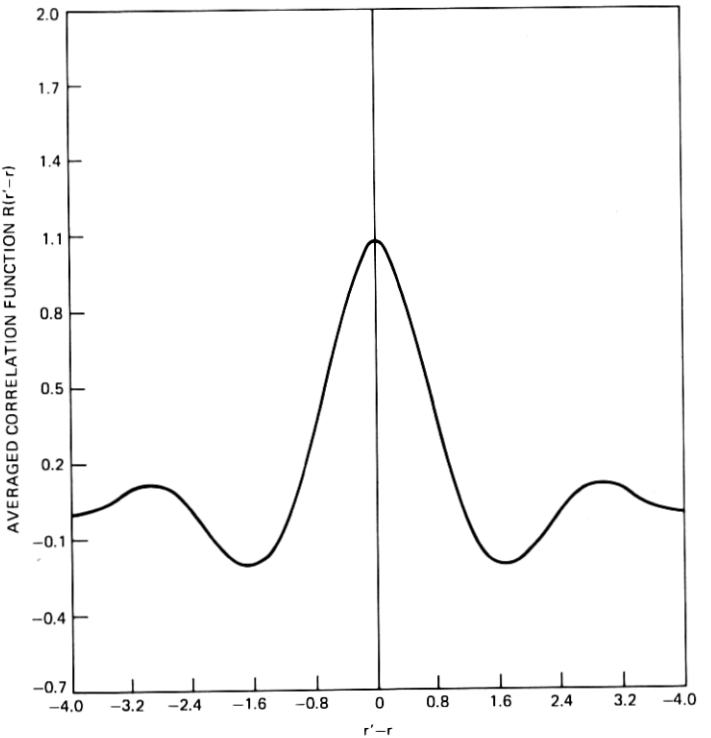

Fig. 6—Averaged autocorrelation function. The average is taken over r in the interval $1 \leq r \leq 5$.

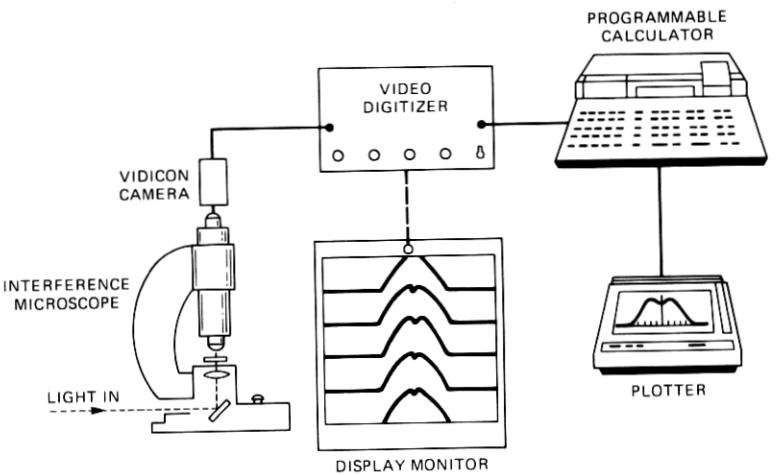

Fig. 7—Experimental arrangement to perform automatic index profiling of whole fibers.

Hewlett Packard 9825A computer with the least significant bit of the Y address serving as the field selector.

The digitizer normally operates by deriving horizontal (line) and vertical (field) timing from the video input signal and uses these timing signals to keep track of the position of the video signal relative to the TV raster at any instant. This location is compared with the selected X, Y sample point and, when coincidence is achieved, the video at that point is digitally encoded to 8 bits or 256 gray levels and sent to the computer which then issues new X, Y coordinates and the procedure is repeated. We have found, however, that the transition of the computer between issuing new data (writing-mode) and receiving the digitized information (reading-mode) is sufficiently long (~3 ms) that it does not allow for the digitization of all Y values for a given X coordinate (one column) within one field, 1/60 s. To do this requires an execution time of 50 μs or less. In fact, only one point per field can be processed, and digitizing a single column typically takes about 3 s. This is not normally a serious limitation since only on the order of 50 columns (requiring 2½ minutes) are needed to measure the profile with good resolution. However, if it is desired to obtain maximum sensitivity by averaging over many scans to reduce video noise levels, this limitation becomes prohibitive.

The computer, on the other hand, is capable of reading 400,000 words of data per second and if it could be freed of the need to supply consecutive Y addresses, digitization of a column could be accomplished in 1/60 s (for each field), saving a factor of almost 200 in time.

This has been achieved with the addition of the interface board shown schematically in Fig. 8, which essentially contains an 8-bit programmable counter and support logic gates. At the start of each columnar digitization, the computer loads the counter with the logic value of the number of points desired and issues the initial X value. These readings are then taken, and a stop pulse is issued. An enable pulse whose length is related to the number of data points is also generated by the circuitry to supply handshaking (timing) for the system and to allow the region being processed to be observed on a display monitor.

A photograph of the display showing a typical graded-index fiber observed at a wavelength of $\lambda = 0.9$ μm is seen in Fig. 9. Location of the point being encoded is indicated by a dot cursor and the gray scale value for all Y elements along a sample line at the selected X position is displayed as a waveform at the side of the monitor screen. The two vertical lines bounding the waveform display indicate the black and white reference levels which are encoded as 255 and 0, respectively.

The sequence of events for determining the fringe shift as a function of radius, $S(r)$, from which the profile is computed, shall be described with reference to Fig. 9. It is first necessary to choose a desired fringe.

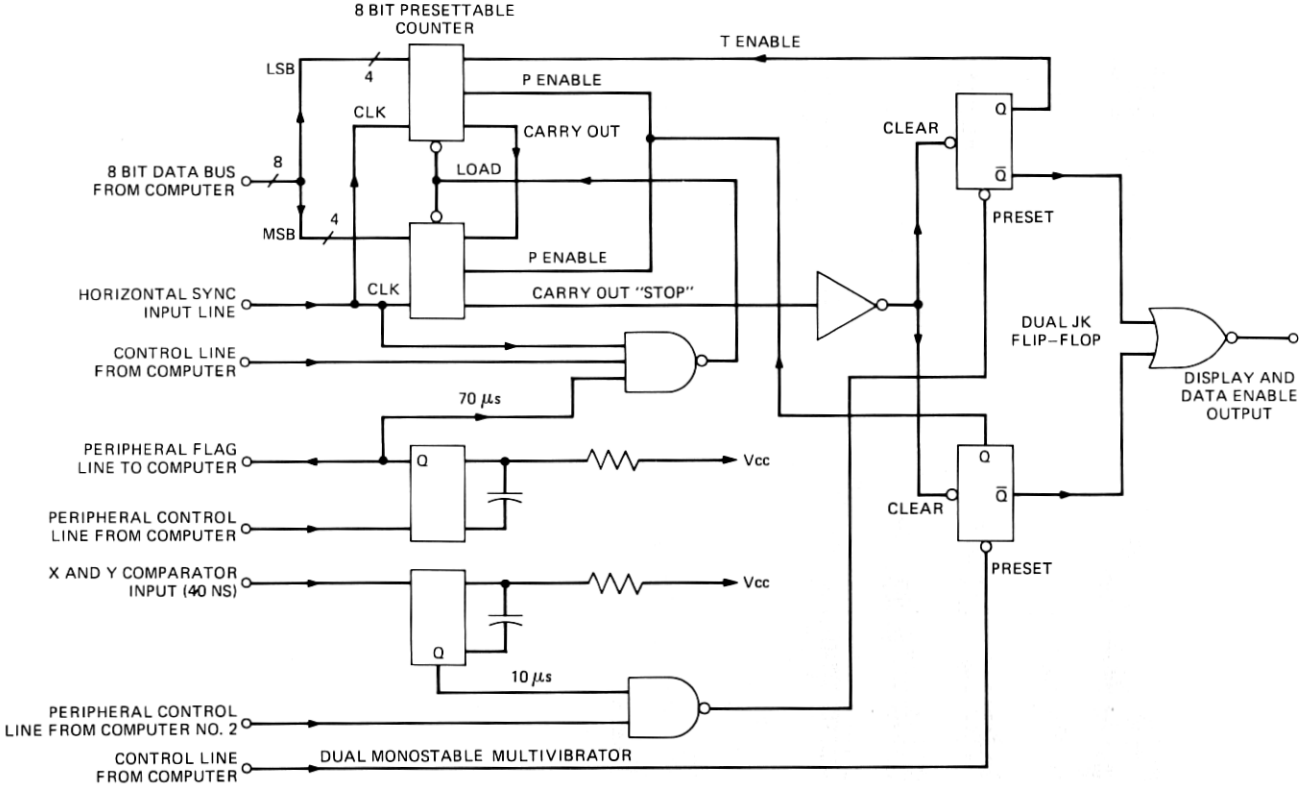

Fig. 8—Video-digitizer interface board to allow data accumulation for each field within one frame time.

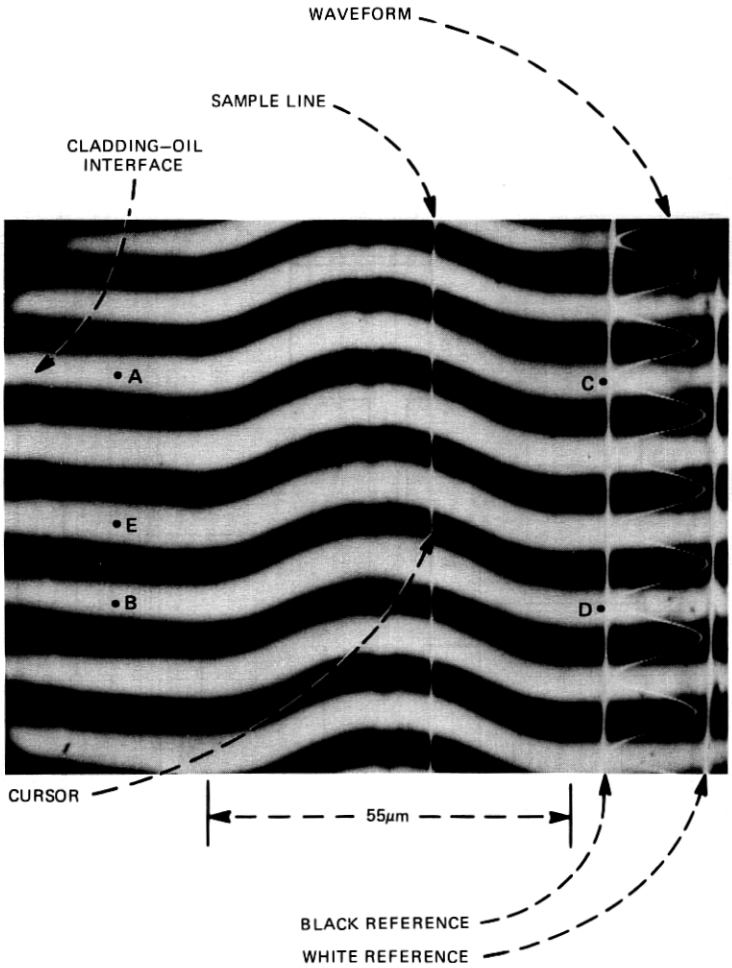

Fig. 9—Display of video monitor showing transversely illuminated whole fiber at a wavelength of 0.9 μm.

This generally is not critical since any fringe should give the same index distribution assuming that the profile is constant along the fiber and the sample is relatively clean and free of surface imperfections. Once selected, the fringe is located by a procedure of fringe counting. For example, starting from point A and proceeding along a line AB, let the desired fringe number be 3. Thus all elements along line AB defined by a fixed X value are digitized. The computer then counts the fringes to find the third one. In this procedure, a fringe is defined by following the digitized data and noting transitions in gray-scale values by more than some fixed number. Twenty data points in the vicinity of the fringe maxima are chosen, and a parabolic fit to them is formed.

The maximum of the curve thus determined is taken as the center of the fringe. The computer also determines at this time the uniform spacing, D, of the fringes in the cladding by locating the center of each fringe and averaging over the number of fringes.

The X position value is then changed and the same determination is made for the right-hand side of the cladding along line CD. A straight line is fitted by the computer to pass through the centers of the third fringe at these right- and left-hand sides. This line serves as the reference level from which fringe displacements are made and also compensates for possible misalignment of the fringes to the scanning line axis.

Next, the X position is automatically set to point E which is about midway between fringe 3 and 4, and scanning proceeds from E to B. X is then incremented for each such columnar encoding and the Y address is automatically corrected to track the fringe by picking midway initial X values as was done for point E.

To enable the calculation of the radius, the XY coordinates of the fiber's axis are located as part of an initial set-up procedure. This is readily achievable due to the index depression which exists along the axis[10] and causes a perceptible dip in the fringes. The initial set-up procedure also includes entering into the computer the coordinates of points A, B, and C, the wavelength of observation, the desired X increment, and the desired fringe number. The computer then takes over and at the end of the encoding process calculates Δn as a function of radius for each half of the core, averages both halves, and plots the resulting index profile along with coordinates and labeling on an XY plotter.

A best-fit power-law (α) curve to the index profile may be determined after the coordinates of the limits over which the fit is to be made are entered. In addition to the α parameter, this fitting procedure also determines the core radius, the shift of the center of the core, the maximum index difference between core and cladding, and a fitting error to provide a measure of how well the α curve approximates the measured profile. These values are then printed out and the best-fit α curve is drawn on the plotter.

Four examples of measured profiles for various GeO_2-doped fibers demonstrating the general applicability of this method are shown in Figs. 10 to 13.

Figures 10 and 11 show typical and reasonably smooth profiles (solid line) which are fit with relatively good α curves (broken lines), the fitting errors being on the order of 1 percent. Perturbations in the profile, mainly in the form of the index depression along the axis and variations in deposition layers close to the center, are clearly resolved. It is important to emphasize that this method assumes circular symmetry for the fiber core and thus variations in core geometry, if

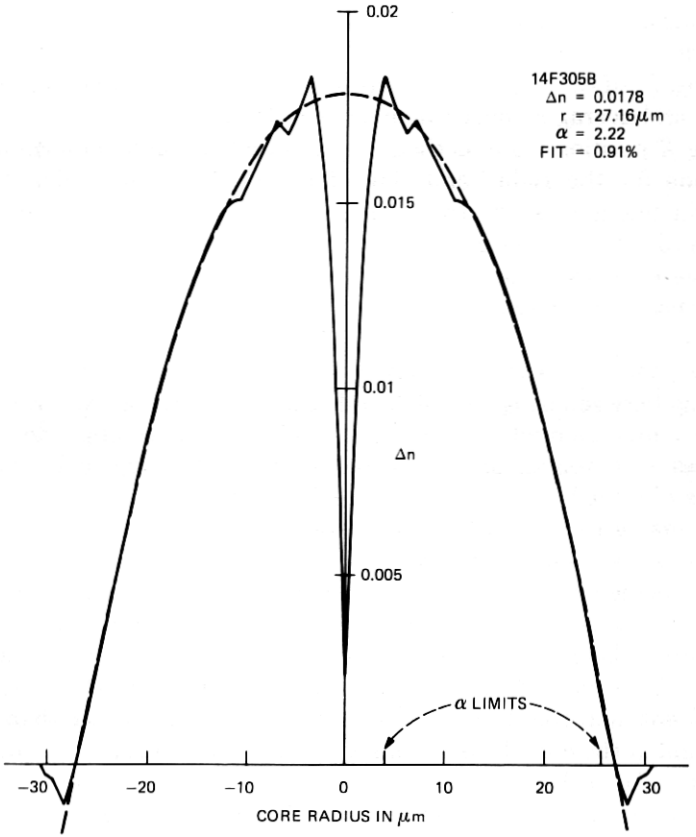

Fig. 10—Profile of typical GeO_2-doped fiber (solid curve) and best-fit α curve (broken curve).

existing, would not be detected. The variations in the plotted profile also represent averages over both sides of the core.

Figure 12 shows the profile of a fiber with strong index variations in the vicinity of the axis, and Fig. 13 shows a fiber with a very large boron barrier layer at the core-cladding interface. These unique features are clearly detectable and well resolved, thus demonstrating the applicability of this technique to even these extreme cases.

We have compared profiles obtained using the circular index analysis technique of Ref. 8, in which the profile is built up piecewise, with the integral equation approach used here. The agreement was excellent with the profiles being essentially identical.

The profiles have also been compared with those obtained by preparing polished slabs of the same fiber samples. The comparison results, presented in detail in Ref. 8, show very good agreement with the average difference of the maximum Δn values and the α values being about 4 percent.

The experimental accuracy of the measured profiles and the effects of index mismatching were investigated by measurements made on unclad fiber (uniform-index) samples under various matched and unmatched conditions. Variations of the index were consistently found to be within about 2 parts in 10^4, in excellent agreement with the theoretical analysis of the previous section. For unclad fibers with intentional index mismatch, we obtained step index profiles with the height of the step corresponding to the degree of mismatch. When a good match is visually observed on the monitor, as evidenced by a straight fringe parallel to the scanning line axis, the error in the profile due to mismatch was found to be on the same order as that due to the index variations (a few parts in 10^4); thus, no attempt at more precise matching was made.

In conclusion, the techniques described to measure the refractive index profiles of optical fibers rapidly and automatically should prove

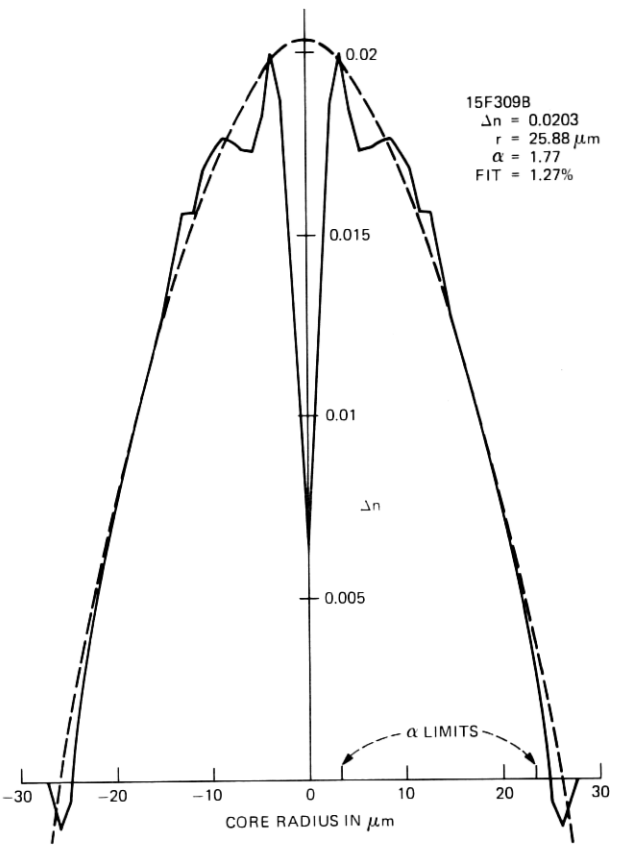

Fig. 11—Profile of GeO_2-doped fiber (solid curve) and best-fit α curve (broken curve) showing somewhat greater variations than fiber of Fig. 10.

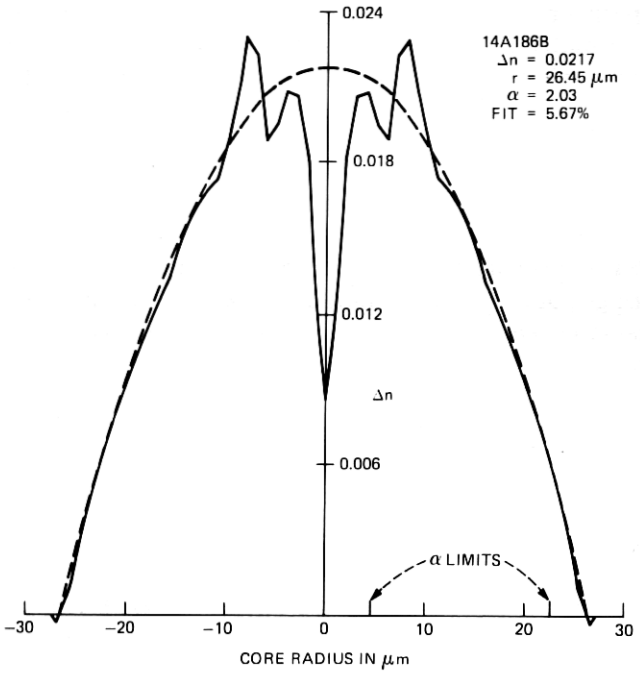

Fig. 12—Profile of GeO_2-doped fiber (solid curve) and best-fit α curve (broken curve) showing strong central index perturbations.

valuable not only in reducing the time required for these measurements but also in forming the basis of an evaluation scheme in which fibers can be rated and selected for specific applications, depending upon the quality of their profiles, almost immediately upon production.

APPENDIX

We sketch the solution of the integral equation (3), which we write in the form

$$\int_y^\infty \frac{xf(x)\,dx}{y\sqrt{(x^2-y^2)}} = g(y). \tag{23}$$

In our application, $f(x)$ is an even function of x; this allows us to express it in the form

$$f(x) = \int_o^\infty F(u)\cos(ux)\,du. \tag{24}$$

Substitution of (24) into (23) yields after integration

$$-\frac{\pi}{2}\int_o^\infty F(u)J_1(uy)\,du = \frac{1}{y}g(y), \tag{25}$$

where J_1 is the Bessel function of order one. This integral relation is the Hankel transform whose inversion is given by the formula

$$F(u) = -\frac{2}{\pi}u\int_o^\infty g(y)J_1(uy)\,dy. \tag{26}$$

Substitution in (24) yields

$$f(x) = -\frac{2}{\pi}\int_o^\infty g(y)\left\{\int_o^\infty u\cos(ux)J_1(uy)\,du\right\}dy. \tag{27}$$

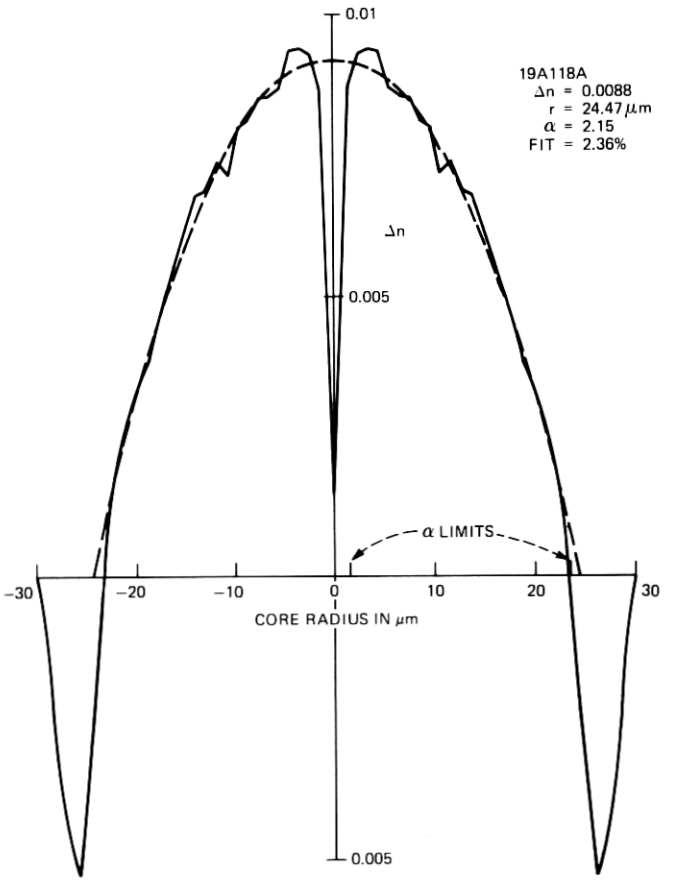

Fig. 13—Profile of GeO_2-doped fiber (solid curve) and best-fit α curve (broken curve) showing resolution of large boron barrier layer.

This expression can also be written in the form:

$$f(x) = \frac{2}{\pi} \int_o^\infty g(y) \left\{ \frac{d}{dy} \int_o^\infty \cos(ux) J_0(uy)\, du \right\} dy. \tag{28}$$

We perform a partial integration

$$f(x)$$

$$= -\frac{2}{\pi} \left\{ g(0) \int_o^\infty \cos(ux)\, du + \int_o^\infty \frac{dg}{dy} \int_o^\infty \cos(ux) J_0(uy)\, du\, dy \right\}, \tag{29}$$

where we used the fact that the fringe shift vanishes outside the fiber core so that $g(\infty) = 0$. The integral over the cosine function vanishes for $x \neq 0$. The integral over the product of the cosine and Bessel functions can be found in tables so that we finally obtain

$$f(x) = -\frac{2}{\pi} \int_x^\infty \frac{dg}{dy} \frac{dy}{\sqrt{y^2 - x^2}}. \tag{30}$$

The integral transform pair (23) and (30) corresponds to the transform pair (3) and (4).

REFERENCES

1. C. A. Burrus and R. D. Standley, "Viewing Refractive-Index Profiles and Small-Scale Inhomogeneities in Glass Optical Fibers: Some Techniques," Appl. Opt., *13* (1974), p. 2365.
2. H. M. Presby, W. Mammel, and R. M. Derosier, "Refractive Index Profiling of Graded Index Optical Fibers," Rev. Sci. Instrum., *47* (1976), p. 348.
3. H. M. Presby and I. P. Kaminow, "Binary Silica Optical Fibers: Refractive Index and Profile Dispersion Measurements," Appl. Opt., *15* (1976), p. 3029.
4. H. M. Presby and H. W. Astle, "Optical Fiber Index Profiling by Video Analysis of Interference Fringes," Rev. Sci. Instr., *49* (1978), p. 339.
5. H. M. Presby, D. Marcuse, and H. W. Astle, "Automatic Refractive Index Profiling of Optical Fibers," Appl. Opt., *17* (1978), p. 2209.
6. B. C. Wonsiewicz, W. G. French, P. O. Lazay, and J. R. Simpson, "Automatic Analysis of Interferograms: Optical Waveguide Refractive Index Profiles," Appl. Opt., *15* (1976), p. 1048.
7. M. E. Marhic, P. S. Ho, and M. Epstein, "Nondestructive Refractive-Index Profile Measurement of Clad Optical Fibers," Appl. Phys. Lett., *26* (1975), p. 574.
8. M. J. Saunders and W. B. Gardner, "Nondestructive Interferometric Measurement of the Delta and Alpha of Clad Optical Fibers," Appl. Opt., *16* (1977), p. 2368.
9. L. M. Boggs, H. M. Presby and D. Marcuse, "Rapid Automatic Index Profiling of Whole Fiber Samples: Part I," B.S.T.J., this issue, pp. 867–882.
10. H. M. Presby, "Axial Refractive Index Depression in Preforms and Fibers," Fiber and Integrated Optics, 2(No. 2).
11. A. M. Yaglom, *An Introduction to the Theory of Stationary Random Functions*, New York: Dover, 1962, p. 23.